with an estimated error bsed on F of 0.13. Plots of $\sum w(|F_o| - |F_c|)^2$ vs. $|F_o|$, reflection order in data collection, $\sin\theta/\lambda$, and various classes of indexes showed no unusual trends.

Acknowledgment. We thank the National Science Foundation (Grant CHE-8219206 to I.P.R.) for financial support of this work and Amoco for a fellowship (to T.W.C.). We also thank the Monsanto Fund and the National Science Foundation for Financial support of the X-ray facilities at Purdue University.

Supplementary Material Available: Complete listings on bond lengths and bond angles, anisotropic thermal parameters, structure factors, and calculated fittings of the observed temperature dependence of the 4-methyl groups of the salt complex to values of δ and J (105 pages). Ordering information given on any current masthead page.

Tungsten as a Weak Backscatterer: An Example of Information Loss in Extended X-ray Absorption Fine Structure (EXAFS) Spectroscopy. Tungsten and Iron EXAFS Studies of Tungsten–Iron–Sulfur Clusters Containing the WS_2Fe Unit

Mark R. Antonio,[1a,b] Boon K. Teo,*[1c] and Bruce A. Averill*[1a,d]

Contribution from AT&T Bell Laboratories, Murray Hill, New Jersey 07974, Department of Chemistry, Michigan State University, East Lansing, Michigan 48824, and Department of Chemistry, University of Virginia, Charlottesville, Virginia 22901. *Received June 11, 1984*

Abstract: The W L_3-edge and Fe K-edge transmission EXAFS (extended X-ray absorption fine structure) spectra of the binuclear complex ions $[S_2WS_2FeX_2]^{2-}$ (**1**, X = SPh; **2**, X = Cl, **3**, X = OPh; Et_4N^+ salts; and **4**, $X_2 = S_5$; Ph_4P^+ salt), the trinuclear complex ions $[S_2WS_2FeS_2Fe(S\text{-}p\text{-}C_6H_4CH_3)_2]^{3-}$ (**5**, Et_4N^+ salt) and $[Cl_2FeS_2WS_2FeCl_2]^{2-}$ (**6**, Ph_4P^+ salt), and the W L_3-edge transmission EXAFS spectrum of tetrathiotungstate, $[WS_4]^{2-}$ (**7**, NH_4^+ salt), have been measured and interpreted. The structural parameters and parameter correlation curves obtained from the FABM (fine adjustment based on models) analysis of the W and Fe EXAFS data for the WS_2Fe complex anions (**1-6**, this work) closely parallel those from the FABM analysis of the Mo and Fe EXAFS data for the MoS_2Fe cluster anion analogues. An important aspect of the present study is the near-absence of the Fe–W peak in the Fourier transforms of the Fe EXAFS data for **1-6**. This represents a type of *information loss* in EXAFS spectroscopy and points to the fact that, in sharp contrast to the principles of X-ray diffraction, the general assumption that heavier elements are stronger backscatterers than lighter ones does not always hold true in EXAFS spectroscopy. This observation is explained in terms of the shape of the W backscattering amplitude profile; there are two minima in the W backscattering amplitude function at ca. 5 and 10 Å^{-1} over the photoelectron wavevector (k) range of practical importance ($3 \lesssim k \lesssim 15$ Å^{-1}). For systems that contain tungsten neighbors in the vicinity of the X-ray absorbing atom, the tungsten peak may be enhanced by extending the data out to high k values ($k > 15$ Å^{-1}) and/or by reducing the Debye–Waller factor by data collection at low temperatures. It is suggested that weak EXAFS backscatterers be avoided in heavy-atom substitution studies, especially for dilute biological systems.

Although the chemistry of synthetic metal–sulfur clusters of the group 6 transition elements molybdenum and tungsten is similar, significant differences are observed when nitrogenase-producing organisms are grown on tungstate in place of molybdate.[2,3] Growth under such conditions renders the nitrogenase system extremely unstable and nonfunctional for the reduction of dinitrogen.[2,3] The putative WFe analogue of the MoFe protein of nitrogenase is presumably either unstable or possesses properties that are incompatible with the function of the metalloenzyme. In view of the inability of tungsten to participate in a functional nitrogenase, the tungsten analogues of several synthetic Mo–Fe–S cluster anions containing the $MoFe_3S_4$ cubane core and the MoS_2Fe core have been prepared and characterized.[4-7] Comparisons of the properties and structures of W–Fe–S clusters containing the WFe_3S_4 and WS_2Fe units to those of the corresponding Mo–Fe–S clusters containing the $MoFe_3S_4$ and MoS_2Fe units (which represent potential structural fragments of the MoFe protein and FeMo cofactor of nitrogenase) are thus of appreciable interest. We report here the results of the W L_3-edge and Fe K-edge transmission EXAFS (extended X-ray absorption fine structure) studies of binuclear complex ions $[S_2WS_2FeX_2]^{2-}$ (**1**, X = SPh,[8a,b] **2**, X = Cl;[7,8a,c,9] **3**, X = OPh;[8a,b] Et_4N^+ salts; and

Chart I

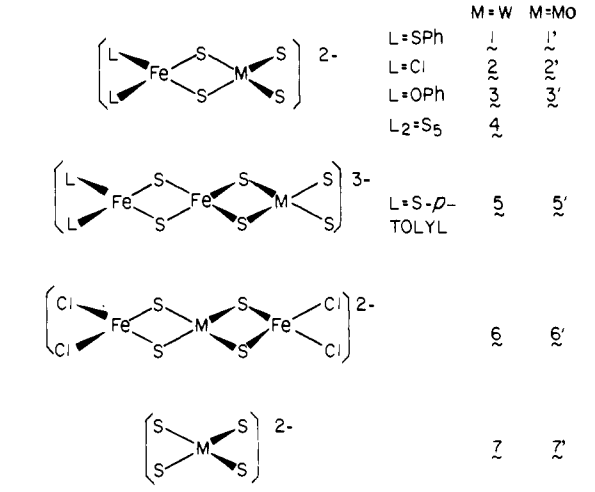

(1) (a) Michigan State University, Department of Chemistry, East Lansing, Michigan 48824. (b) Current address: The Standard Oil Company (Ohio), Warrensville Research Center, Cleveland, Ohio 44128. (c) AT&T Bell Laboratories, Murray Hill, New Jersey 07974. (d) Current address: University of Virginia, Department of Chemistry, Charlottesville, Virginia 22901.

(2) Benemann, J. R.; Smith, G. M.; Kostel, P. J.; McKenna, C. E. *FEBS Lett.* **1973**, *29*, 219.

(3) Nagatani, H. H.; Brill, W. J. *Biochim. Biophys. Acta* **1974**, *362*, 160.

(4) Averill, B. A. *Struct. Bonding (Berlin)* **1983**, *53*, 59.

(5) Holm, R. H. *Chem. Soc. Rev.* **1981**, *10*, 455.

(6) Müller, A.; Diemann, E.; Jostes, R.; Bögge, H. *Angew. Chem., Int. Ed. Engl.* **1981**, *20*, 934.

(7) Coucouvanis, D. *Acc. Chem. Res.* **1981**, *14*, 201.

0002-7863/85/1507-3583$01.50/0

4, $X_2 = S_5$;[10a] Ph_4P^+ salt), the trinuclear complex ions $[S_2WS_2FeS_2Fe(S\text{-}p\text{-}C_6H_4CH_3)_2]^{3-}$[8c] (**5**, Et_4N^+ salt), and $[Cl_2FeS_2WS_2FeCl_2]^{2-}$[10b,c] (**6**, Ph_4P^+ salt) and the W EXAFS of tetrathiotungstate, WS_4^{2-}[11] (**7**, NH_4^+ salt). We note that the structure of **5** has not been determined by single-crystal X-ray diffraction. In addition, EXAFS provides, for the first time, separate W–S (terminal), W–S (bridging), Fe–S (bridging), and Fe–Cl (terminal) distances for the crystallographically disordered dianion **2** (only average M–X (terminal) and M–S (bridging) distances, where M = (W + Fe)/2 and X = (Cl + S)/2, are available from X-ray crystallography). The present results for the WS_2Fe complex anions (**1**–**7**, cf. Chart I) are also compared to those of the MoS_2Fe cluster anion analogues (**1′**–**7′**) discussed in detail elsewhere.[12]

Interestingly, tungsten is a much weaker backscatterer than molybdenum in that the Fe–W peaks in the Fourier transforms for the Fe EXAFS data of **1**–**6** are much smaller than the Fe–Mo peaks in the Fourier transforms for the Fe EXAFS data of **1′**–**6′**, despite the fact that tungsten is a heavier element than molybdenum. This observation is explained in terms of the two minima (k = 5 and 10 Å^{-1}) in the tungsten backscattering amplitude[13] over the k range of importance (3–15 Å^{-1}). The diminution of the Fe–M backscattering component upon replacing M = Mo with M = W in the FeS_2M cores of **1**–**6** represents a type of information loss in EXAFS spectroscopy and illustrates the danger in the general assumption that heavier elements are inherently stronger backscatterers than lighter elements. To enhance the tungsten signal, one may have to extend the data to high k regions (>15 Å^{-1}) and/or minimize the Debye–Waller factor by performing the experiments at low temperatures.

Experimental Section

Materials. Compounds $(Et_4N)_2[S_2WS_2FeX_2]$ (**1**, X = SPh;[8a,b] **2**, X = Cl;[8a,c,9] **3**, X = OPh[8a,b]), $(Et_4N)_3[S_2WS_2FeS_2Fe(S\text{-}p\text{-}C_6H_4CH_3)_2]$[8c] (**5**), and $(NH_4)_2[S_2WS_2]$[11] (**7**) were prepared according to literature methods and were provided by Drs. H. C. Silvis and R. H. Tieckelmann. The clusters $(Ph_4P)_2[S_2WS_2FeS_5]$[10a] (**4**) and $(Ph_4P)_2[Cl_2FeS_2WS_2FeCl_2]$[10b,c] (**6**) were kindly supplied by Prof. D. Coucouvanis.

The Fe and W transmission EXAFS experiments were performed on pressed boron nitride pellet samples as described previously.[12] The sample concentration and thickness were adjusted such that the edge jump was approximately equal to 1. The cells (sample volume: (1–3) × 3 × 19 mm^3) were sealed with 1 mil Kapton tape and were kept under an inert atmosphere until just prior to measurements.

X-ray Absorption Measurements. The iron K-edge and tungsten L_3-edge transmission X-ray absorption measurements for **1**–**6** and **1**–**3**, **5**, and **6**, respectively, were performed at ambient temperature at the Cornell High Energy Synchrotron Source[14a] (CHESS) on the C2[15] EXAFS beam line. The tungsten L_3-edge transmission X-ray absorption measurements for **4** and **7** were performed at ambient temperature at the Stanford Synchrotron Radiation Laboratory[14b] (SSRL) on beam line I-5.[15] Figures of the raw X-ray absorption data, in the form ln (I_0/I) vs. E (in eV) for **1**–**7** are presented in the supplementary material along with the background-subtracted iron and tungsten EXAFS spectra, $k^3\chi(k)$ vs. k (in Å^{-1}). The data reduction[16,17] and curve fitting[18] were performed as detailed elsewhere.[12,19]

(8) (a) Silvis, H. C.; Tieckelmann, R. H.; Cleland, W. E.; Holtman, D. A.; Ward, D. L.; Averill, B. A., to be submitted for publication. (b) Silvis, H. C. Ph.D. Dissertation, Michigan State University, East Lansing, Michigan, 1981. (c) Tieckelmann, R. H. Ph.D. Dissertation, Michigan State University, East Lansing, Michigan, 1982.

(9) (a) Müller, A.; Tölle, M. G.; Bögge, H. *Z. Anorg. Allg. Chem.* **1980**, *471*, 115. (b) Müller, A.; Jostes, R.; Tölle, M. G.; Trautwein, A.; Bill, E. *Inorg. Chim. Acta* **1980**, *46*, L121.

(10) (a) Coucouvanis, D.; Stremple, P.; Simhon, E. D.; Swenson, D.; Baenziger, N. C.; Draganjac, M.; Chan, L. T.; Simopoulos, A.; Papaefthymiou, V.; Kostikas, A.; Petrouleas, V. *Inorg. Chem.* **1983**, *22*, 293. (b) Coucouvanis, D.; Baenziger, N. C.; Simhon, E. D.; Stremple, P.; Swenson, D.; Simopoulous, A.; Kostikas, A.; Petrouleas, V.; Papaefthymiou, V. *J. Am. Chem. Soc.* **1980**, *102*, 1732. (c) Coucouvanis, D.; Simhon, E. D.; Stremple, P.; Ryan, M.; Swenson, D.; Baenziger, N. C.; Simopoulos, A.; Papaefthymiou, V.; Kostikas, A.; Petrouleas, V. *Inorg. Chem.* **1984**, *23*, 741.

(11) (a) Krüss, G. *Justus Liebigs Ann. Chem.* **1884**, *225*, 1. (b) Sasvari, K. *Acta Crystallogr.* **1963**, *16*, 719.

(12) Teo, B.-K.; Antonio, M. R.; Averill, B. A. *J. Am. Chem. Soc.* **1983**, *105*, 3751.

(13) Teo, B.-K.; Lee, P. A. *J. Am. Chem. Soc.* **1979**, *101*, 2815.

(14) (a) CHESS was operated in a mode parasitic to high energy physics experiments with the Cornell Electron Storage Ring (CESR) at the Wilson Laboratory of Cornell University, Ithaca, New York. Typically, CESR operated at 5.18 GeV with approximately 4 to 12 mamps of electron beam current. (b) SSRL utilized the synchrotron radiation obtained from the dedicated operation of the Stanford Positron Electron Annihilator Ring (SPEAR) at the Stanford Linear Accelerator Center (SLAC) of Stanford University, Stanford, CA. SPEAR operated at 2.98 GeV with between 40 and 70 mamps of electron beam current.

(15) (a) The white synchrotron radiation from CESR and SPEAR was monochromated by channel-cut silicon ⟨220⟩ crystals. Prior to each scan, the monochromator was detuned by 50% to reduce the harmonic-to-functional beam intensity ratio. The incident (I_0) and transmitted (I) beam intensities were monitored with flow-type ionization chambers with a combination of nitrogen (I_0) and argon (I) detecting gases at both the Fe and W edges. I_0 and I were typically recorded with an integration time of 1–2 s/point by constant I_0 accumulation, to compensate for the time decay of the incident intensity (with a DEC LSI microcomputer), and by constant time accumulation for I_0 and I (with a DEC PDP 11/03 minicomputer) at CHESS and SSRL, respectively. The photon energy was scanned from about 100 eV below to about 900 eV above the iron K-photoabsorption and tungsten L_3-photoabsorption edges. Each absorption spectrum recorded at CHESS contained between 205 and 218 data points at discrete energy increments in steps of constant k (Å^{-1}), the photoelectron wavevector. The incremental energy steps ranged from 2 to 7 eV/point at the beginning and at the end of each scan. The data recorded at SSRL were obtained in discrete monochromator steps of constant energy (ca. 2.0 eV/point); approximately 450 points were collected for each spectrum. The energy resolution near the tungsten L_3-edge (10206.8 eV)[15b] on both beam lines 1-5 and C2 was ca. 5 eV, and that near the iron K-edge (7112.0 eV)[15b] on C2 was ca. 2 eV. (b) Bearden, J. A.; Burr, A. F. *Rev. Mod. Phys.* **1967**, *39*, 125.

(16) For conversion to k space ($k = [(2m/\hbar^2)(E - E_0^{exptl})]^{1/2}$) the experimental energy thresholds (E_0^{exptl}, in eV) were chosen at 10210 for the W data of **1**, **2**, and **6**, 10206 for **3** and **5**, 10178 for **4** and **7**, and 7130 for all Fe data. The edge position energies [E_0^P, the photon energy (in eV) at half-height of the edge jump] for the W and Fe data were determined to be respectively the following: 10197 and 7114 (**1**); 10197 and 7115 (**2**); 10193 and 7115 (**3**); 10164 and 7114 (**4**); 10193 and 7114 (**5**); 10198 and 7115 (**6**); and 10164 (**7**). The data were weighted by k^3, and the background was removed by using five sets (ca. 2.83 Å^{-1} each) of cubic spline functions. The EXAFS was normalized by dividing by the edge jumps (which ranged from ca. 0.5 to 1.8 for the W data and from 0.4 to 0.7 for the Fe data for **1**–**7**) and also corrected for the falloff in the absorption cross section according to Victoreen's equation.[17] No thickness effect corrections were applied to the EXAFS data described herein.

(17) (a) An absorption falloff correction was applied according to[17b] $\mu_0/\rho = C\lambda^3 - D\lambda^4$, in which μ_0/ρ is the mass absorption coefficient, λ is the wavelength of the incident X-radiation, and the parameters C and D (associated with the X-ray absorbing atom) are[17c] respectively 126 and 27.2 for Fe and 65.3 and 11.9 for W. Since accurate values for the Victoreen coefficients C and D in the range of X-ray wavelengths $\lambda_{L_2} < \lambda < \lambda_{L_3}$ encountered in W L_3-edge EXAFS measurements are not available, the C (65.3) and D (11.9) values[17c] between the specified wavelength limits $\lambda_{L_3} < \lambda < \lambda_{M_1}$ were used in the correction calculations. (b) Victoreen, J. A. *J. Appl. Phys.* **1948**, *19*, 855. (c) Macgillavry, C. H., Rieck, G. D., Lonsdale, K., Eds. "International Tables for X-ray Crystallography"; Kynoch Press: Brimingham, England, 1968; Vol. III, pp 171–173.

(18) (a) A least-squares minimization technique which incorporates Marquardt's scheme[18b] for iterative estimation of nonlinear least-squares parameters was used to curve fit the Fourier filtered spectra with eq 1. The nonlinear least-squares refinements of the scale factors (independent of the photoelectron wavevector k_j) for the scattering atoms of the jth type, B_j, at distances r_j from the absorbing atom, the root-mean-square relative displacements σ_j (Debye–Waller factors), along r_j, and the threshold energy differences, ΔE_{0j}, were based upon the minimization of the sum of squares of the residuals, $\Sigma^2 = \sum_i [k^3\chi(k)_i - k^3\chi'(k)_i]^2$. $k^3\chi(k)$ and $k^3\chi'(k)$ are the calculated and the observed EXAFS, respectively, and i runs through each data point. (b) Marquardt, D. W. *J. Soc. Ind. Appl. Math.* **1963**, *11*, 431. (c) Sayers, D. E.; Lytle, F. W.; Stern, E. A. In "Advances in X-ray Analysis"; Henke, B. L., Newkirk, J. B., Mallett, R. G., Eds.; Plenum Press: New York, 1970; Vol. 13, pp 248–271. (d) Sayers, D. E.; Stern, E. A.; Lytle, F. W. *Phys. Rev. Lett.* **1971**, *27*, 1204. (e) Stern, E. A. *Phys. Rev. B* **1974**, *10*, 3027. (f) Lytle, F. W.; Sayers, D. E.; Stern, E. A. *Phys. Rev. B* **1975**, *11*, 4825. (g) Ashley, C. A.; Doniach, S. *Phys. Rev. B* **1975**, *11*, 1279. (h) Lee, P. A.; Pendry, J. B. *Phys. Rev. B* **1975**, *11*, 2795. (i) Kincaid, B. M.; Eisenberger, P. *Phys. Rev. Lett.* **1975**, *34*, 1361. (j) Lee, P. A.; Beni, G. *Phys. Rev. B.* **1977**, *15*, 2862. (k) Lee, P. A.; Citrin, P. H.; Eisenberger, P.; Kincaid, B. M. *Rev. Mod. Phys.* **1981**, *53*, 769.

(19) (a) Antonio, M. R.; Teo, B.-K.; Cleland, W. E.; Averill, B. A. *J. Am. Chem. Soc.* **1983**, *105*, 3477. (b) Teo, B.-K.; Antonio, M. R.; Coucouvanis, D.; Simhon, E. D.; Stremple, P. P. *J. Am. Chem. Soc.* **1983**, *105*, 5767. (c) Teo, B.-K.; Chen, H. S.; Wang, R.; Antonio, M. R. *J. Non-Cryst. Solids* **1983**, *58*, 249. (d) Bruck, M. A.; Korte, H.-J.; Bau, R.; Hadjiliadis, N.; Teo, B.-K. In "Platinum, Gold, and Other Metal Chemotherapeutic Agents: Chemistry and Biochemistry"; Lippard, S. J., Ed.; American Chemical Society: Washington, DC, 1983; ACS Symp. Series, pp 245–262. (e) Teo, B.-K. *Acc. Chem. Res.* **1980**, *13*, 412.

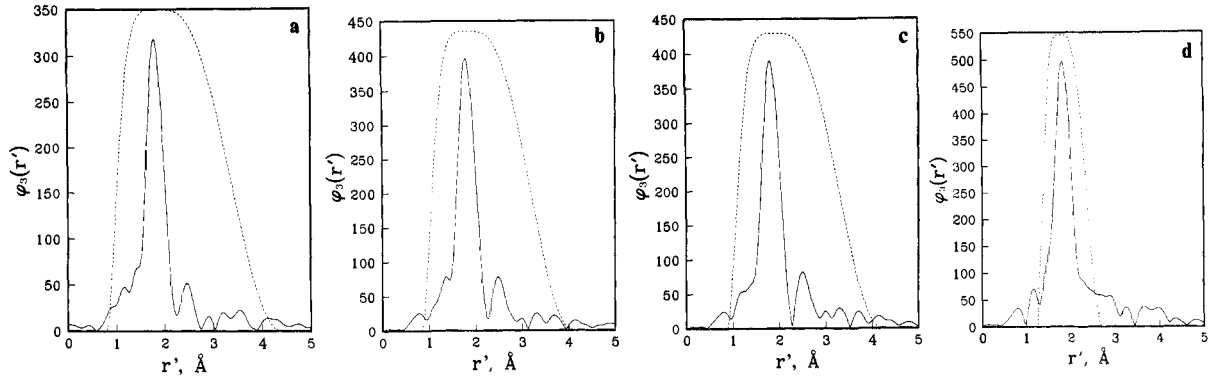

Figure 1. Fourier transforms (solid curves), $\phi_3(r')$ vs. r' (Å; before phase shift correction), of the background-subtracted $k^3\chi(k)$ vs. k tungsten L_3-edge transmission EXAFS data and filtering windows (dashed curves) for (a) $[S_2WS_2Fe(SC_6H_5)_2]^{2-}$ (**1**), (b) $[S_2WS_2Fe(OC_6H_5)_2]^{2-}$ (**3**), (c) $[S_2WS_2FeS_2Fe(S\text{-}p\text{-}C_6H_4CH_3)_2]^{3-}$ (**5**), and (d) $[WS_4]^{2-}$ (**7**).

Results and Discussion

W L_3-Edge Data. Fourier transforms of the normalized and corrected W EXAFS, $k^3\chi(k)$ vs. k, of clusters **1**, **3**, **5**, and **7** are shown as the solid curves in Figure 1a–d.[20a] The Fourier transforms of **1**–**6** exhibit two distinct peaks: the first, intense peak at short distances (ca. 1.7–1.8 Å) is due to backscattering from the neighboring sulfur atoms, and the second, weaker peak at longer distances (ca. 2.3–2.4 Å) is due to backscattering from the neighboring iron atoms. For **7**, the transformed spectrum exhibits only a single peak at ca. 1.8 Å, due to W–S backscattering. The dashed curves shown in Figure 1a–d are the window functions used to filter the W–S and W–Fe backscattering contributions from the distance space (Å) and to Fourier inverse transform the data back to k space (Å^{-1}). The resulting Fourier filtered EXAFS data, $k^3\chi(k)$ vs. k, for **1**, **3**, **5**, and **7** in the region 3–15 Å^{-1} are shown as the solid curves in Figure 2a–d;[20b] they were employed in the nonlinear least-squares curve fitting[18a,b] with the conventional single-scattering formalism[18c-k] (eq 1) of the EXAFS effect with theoretical amplitude $F_j(k)$ and phase $\phi_j(k)$ functions.[13,21] The

$$k^3\chi(k) = \sum_j B_j F_j(k_j) k_j^2 \exp(-2\sigma_j^2 k_j^2) \frac{\sin\,[2k_j r_j + \phi_j(k_j)]}{r_j^2} \qquad (1)$$

filtered EXAFS spectra of **1**–**6** were fit with a two-term formulation[22] (j = S, Fe), and the filtered spectrum of **7** was fit with a single-term formulation[22] (j = S) of the EXAFS effect. The best fits based upon theory, BFBT (dashed curves), and the Fourier filtered data (solid curves) of **1**, **3**, **5**, and **7** are depicted in Figure 2a–d.[20b]

The resulting best-fit (BFBT) least-squares refined parameters and estimated standard deviations (in parentheses) are listed in Table I. Also included in Table I are the restricted fit results (second row of parameters per term) obtained from the nonlinear least-squares refinements with the scale factor ratios B_{Fe}/B_S fixed at the known coordination number ratios (i.e., $B_{Fe}/B_S = 1/4$ for **1**–**5**, and 1/2 for **6**).

The BFBT results were further refined via the fine adjustment based on models (FABM) technique[12] using the characteristic values listed in Table II. The FABM results are tabulated in Table III and compared with crystallographical values. For **5**, a comparison of the structural parameters by EXAFS and single-crystal X-ray diffraction techniques must await the completion of the crystallographic investigation.

The Debye–Waller factors in Tables I and II show that the σ_S values are diagnostic of the structural differences between WS_4 units in **1**–**7**. Thus, clusters **1**–**5** (with $\sigma_S^* = 0.050$ Å) have both bridging and terminal sulfides with nonequivalent distances, while clusters **6** and **7** (with $\sigma_S^* = 0.028$ Å) contain either bridging (**6**) or terminal (**7**) sulfides with equivalent distances. In fact, for **6** and **7**, the EXAFS-determined Debye-Waller factor provides an accurate measure of the average thermal vibrational amplitude (σ_{vib}) of the bound sulfides to tungsten in **1**–**7**. We shall assume $\sigma_{vib} = 0.028$ Å for the W–S bonds in **1**–**7**.[23] Similar observations were also obtained[12] for the molybdenum analogues of clusters **6** and **7**, $[Cl_2FeS_2MoS_2FeCl_2]^{2-}$ and $[MoS_4]^{2-}$, respectively.

With use of a procedure outlined previously,[12] it was possible to determine both the mean terminal and bridging W–S distances from the FABM distances with the aid of the EXAFS-determined Debye–Waller factors. The results are tabulated in Table IV along with the corresponding crystallographic values. It is obvious from Table IV that the EXAFS-derived r_m and r_n are in excellent agreement (ca. ±0.01 Å) with the average bridging (r_b) and terminal (r_t) W–S crystallographic distances, respectively.

The individual terminal and bridging W–S distances for the crystallographically disordered dianion **2** are included in Table IV. Only average M–S (bridging) and M–X (terminal) distances, where M = (W + Fe)/2 and X = (S + Cl)/2, are available from single-crystal X-ray diffraction methods[7,9a] due to the twofold

(20) (a) The Fourier transforms of the EXAFS data for clusters **2**, **4**, and **6** are available as supplementary material (Figure X1Va-c for the W EXAFS and Figure XVa–c for the Fe EXAFS). (b) The Fourier filtered EXAFS data, $k^3\chi(k)$ vs. k, and the nonlinear least-squares best fits, based on theoretical functions, to the filtered EXAFS of **2**, **4**, and **6** are available as supplementary material (Figures XVIa–c for the W EXAFS and Figures XVIIa–c for the Fe EXAFS).

(21) (a) The total phase function for a particular absorber–backscatterer combination was obtained as the sum of the individual absorber (ϕ_M^a; M = W, Fe) and the backscatterer (ϕ_j^b; j = O, S, Fe, W) phase functions, $\phi_j = \phi_M^a + \phi_j^b - \pi$. The factor of π is included for K-edge (Fe) EXAFS only and is not included in the L_3-edge (W) total phase function. For each k value in the experimental EXAFS spectrum, $k^3\chi(k)$ vs. k, $\phi(k)$, and $F(k)$ were interpolated from the theoretical values[21b] with cubic functions. (b) The theoretical values of the EXAFS functions, calculated at discrete intervals in k (Å^{-1}) space, were obtained from ref 13: from Tables VII and VIII for the central atom phases ϕ_{Fe}^a and ϕ_W^a, respectively (calculated by using Herman–Skillman wave functions); from Table II for the back-scattering phases ϕ_S^b and ϕ_{Fe}^b (calculated by using Clementi–Roetti wave functions); from Table V for the back-scattering phases ϕ_{Cl}^b and ϕ_W^b (calculated by using Herman–Skillman wave functions); from Table I for the back-scattering amplitudes F_S and F_{Fe} (calculated by using Clementi–Roetti wave functions); from Table IV for the back-scattering amplitudes F_{Cl} and F_W (calculated by using Herman–Skillman wave functions). Oxygen phase ϕ_O^b and amplitude F_O functions (calculated by using Herman–Skillman wave functions) were obtained from the following: Teo, B.-K. *J. Am. Chem. Soc.* **1981**, *103*, 3990 (Table II supplementary material, for $\beta = 180°$).

(22) To fit a single term, four parameters were varied in the nonlinear least-squares curve-fitting procedure: a scale factor, B_j (the scale factor is related to the number of neighbors N_j by $B_j = S_j N_j$, where S_j is the amplitude reduction factor); a Debye–Waller factor, σ_j; an interatomic distance, r_j; and a threshold energy difference, ΔE_{0j}. Similarly, to fit two and three terms, eight and twelve parameters, respectively, were varied in the nonlinear least-squares curve-fitting procedure.

(23) The vibrational contribution to the Debye-Waller factor σ_{vib} (in Å) can also be calculated in a diatomic approximation[24,25] according to $\sigma_{vib} = 3.151 \times 10^{-3}\,[(\mu/K)\coth(x/2)]^{1/2}$. In this treatment, K is the force constant, x is equal to $1.441\nu/T$, and T is the temperature in K. Using the vibrational frequency $\nu = 465$ cm^{-1}, and the approximate force constant $K = 3.58$ mdyn/Å[26] yields $\sigma_{vib} = 0.0399$ Å at $T = 298$ K for the W–S bonds in **7**. This value is in good agreement with that of 0.0452 Å calculated in a more exact treatment by Müller and Nagarajan[27] and is somewhat higher than the EXAFS result of 0.028 Å for **7**. The origin of this discrepancy is not clear. Nevertheless, as long as we consistently use the same $\sigma_{vib} = 0.028$ Å for compounds **1**–**7**, the resulting σ_{stat} values should accurately reflect the static (structural) disorder.

Table I. The BFBT Least-Squares Refined Interatomic Distances (r, Å), Debye–Waller Factors (σ, Å), and Coordination Numbers (N) with Estimated Standard Deviations (in Parentheses), Energy Threshold Differences (ΔE_0^P, eV), and Scale Factors (B) for the W L_3-Edge and the Fe K-Edge Transmission EXAFS of Complexes **1**–**7**, along with Available Single-Crystal X-ray Diffraction Results

		distance				amplitude[c]	
		EXAFS		diffraction[a]		EXAFS	
ompd	term	ΔE_0^{P}[b]	r	r	% error	σ	B
1	W–S	14.38	2.207 (13)	2.202 (2)	0.2	0.048 (14)	1.548
		13.01[d]	2.203[d]			0.046[d]	1.457[d]
	W–Fe	−11.89	2.696 (43)	2.772 (1)	−2.7	0.045 (39)	0.231
		−21.28[d]	2.665[d]			0.063[d]	0.364[d]
1	Fe–S	9.51	2.308 (18)	2.297 (2)	0.5	0.055 (18)	1.943
		9.43	2.307			0.054	1.869
	Fe–W	−6.61	2.766 (46)	2.772 (1)	−0.2	0.002 (58)	0.183
		−0.17	2.780			0.054	0.467
2	W–S	14.79	2.208 (10)			0.045 (10)	1.782
		14.86	2.209			0.045	1.788
	W–Fe	−6.36	2.749 (37)	2.808 (2)	−2.1	0.071 (23)	0.479
		−5.99	2.751			0.069	0.447
2	Fe–S/Cl	6.62	2.285 (22)			0.061 (16)	2.167
		7.25	2.286			0.062	2.202
	Fe–W	−27.02	2.744 (70)	2.808 (2)	−2.3	0.049 (65)	0.178
		−22.05	2.758			0.079	0.552
3	W–S	14.27	2.207 (16)	2.203 (11)	0.2	0.049 (16)	2.031
		14.87	2.209			0.049	2.022
	W–Fe	−10.09	2.716 (60)	2.794 (2)	−2.8	0.088 (32)	0.822
		−7.62	2.729			0.072	0.506
3	Fe–S	15.87	2.351 (28)	2.307 (3)	1.9	0.035 (34)	0.599
		15.71	2.350			0.029	0.548
	Fe–W	3.41	2.825 (63)	2.794 (2)	1.1	0.040 (40)	0.164
		4.30	2.826			0.058	0.274
	Fe–O	−3.17	1.862 (32)	1.890 (7)	−1.5	0.000 (38)	0.538
		−3.36	1.862			0.000	0.548
4	W–S	11.63	2.203 (16)	2.206 (8)	−0.1	0.052 (17)	1.692
		11.69	2.203			0.053	1.691
	W–Fe	−8.64	2.717 (40)	2.753 (3)	−1.3	0.000 (48)	0.222
		−4.79	2.729			0.052	0.423
4	Fe–S	10.03	2.307 (18)	2.295 (9)	0.5	0.053 (17)	1.801
		10.16	2.307			0.053	1.748
	Fe–W	−4.85	2.756 (35)	2.753 (3)	0.1	0.025 (25)	0.232
		−2.94	2.761			0.051	0.437
5	W–S	15.47	2.217 (16)			0.045 (20)	1.924
		15.96	2.218			0.044	1.904
	W–Fe	−6.47	2.732 (80)			0.091 (46)	0.814
		−2.64	2.755			0.072	0.476
5	Fe–S	6.41	2.251 (31)			0.074 (21)	1.814
	Fe–W	15.26	2.786 (16)			0.090 (9)	0.368
		15.49	2.792			0.071	0.178
	Fe–Fe	17.82	2.802 (23)			0.086 (18)	0.319
		18.62	2.795			0.096	0.355
6	W–S	14.61	2.222 (8)	2.209 (5)	0.6	0.020 (20)	1.858
		14.43	2.221			0.019	1.839
	W–Fe	−1.35	2.761 (33)	2.801 (9)	−1.4	0.061 (24)	0.722
		−1.36	2.761			0.070	0.919
6	Fe–S/Cl	4.05	2.266 (25)	2.280 (5)	−0.6	0.063 (20)	1.946
	Fe–W	7.54	2.821 (65)	2.801 (9)	0.7	0.074 (15)	0.487
7	W–S	17.39	2.210 (9)	2.17 (1)	1.8	0.026 (22)	1.918

[a] The single-crystal X-ray diffraction data were obtained from ref 8a for **1** and **3** and ref 9a, 10a, 10c, and 11b for **2**, **4**, **6**, and **7**, respectively. [b] These standardized energy threshold differences ΔE_0^P were obtained according to $\Delta E_0^P = \Delta E_0 + E_0^{expt} - E_0^P$. Here ΔE_0 was the least-squares refined energy threshold difference, E_0^{expt} was the experimentally chosen energy threshold,[16] and E_0^P was the edge position energy.[16] [c] The coordination numbers via the FABM method are given in Table III. [d] Throughout this table, the parameters in the second row within each term were obtained from a restricted fit with the ratio of the scale factors for the two backscattering terms fixed at the known value.

disorder of the dianion **2**, which is located on a center of symmetry. The advantage of EXAFS is that it is an element-specific spectroscopic technique that can be used to probe separately the local structures around the W and the Fe atoms.

Fe K-Edge Data. Fourier transforms of the iron EXAFS data of **1**, **3**, and **5** are shown in Figure 3a–c (solid curves).[20a] Each Fourier transform exhibits an intense peak at ca. 1.8 Å, which is due to backscattering by the neighboring sulfur (**1**, **3**–**5**) and sulfur and chlorine (**2**, **6**) atoms about iron. The transformed data of **3** (Figure 3b) also show an intense peak at ca. 1.4 Å, due to Fe–O backscattering. Figure 3a–c exhibits very small peaks at ca. 2.5–2.7 Å, which are interpreted as being due to backscattering contributions from tungsten (**1**–**4**, **6**) and tungsten/iron (**5**) atoms in the local environment about iron in each cluster.

The magnitude of the Fe–W Fourier transform peaks in **1**–**4** and **6** (each with one tungsten neighbor to iron) and **5** (with an average of one-half tungsten and one iron neighbor per iron) is approximately 50% less than that of the corresponding Fe–Mo Fourier transform peaks in the analogous Mo–Fe–S clusters.[28,29a]

(24) Cyvin, S. J. "Molecular Vibrations and Mean Square Amplitudes"; Elsevier: Amsterdam, 1968; p 71.
(25) Teo, B. K. In "EXAFS Spectroscopy: Techniques and Applications"; Teo, B. K., Joy, D. C., Eds.; Plenum: New York, 1981; p 19.
(26) Müller, A.; Krebs, B. *J. Mol. Spectros.* **1967**, *24*, 180.
(27) Müller, A.; Nagarajan, G. *Z. Naturforsch.* **1966**, *21B*, 508.
(28) (a) Antonio, M. R. Ph.D. Dissertation, Michigan State University, East Lansing, Michigan, 1983. (b) Antonio, M. R.; Teo, B.-K.; Averill, B. A., to be submitted for publication.

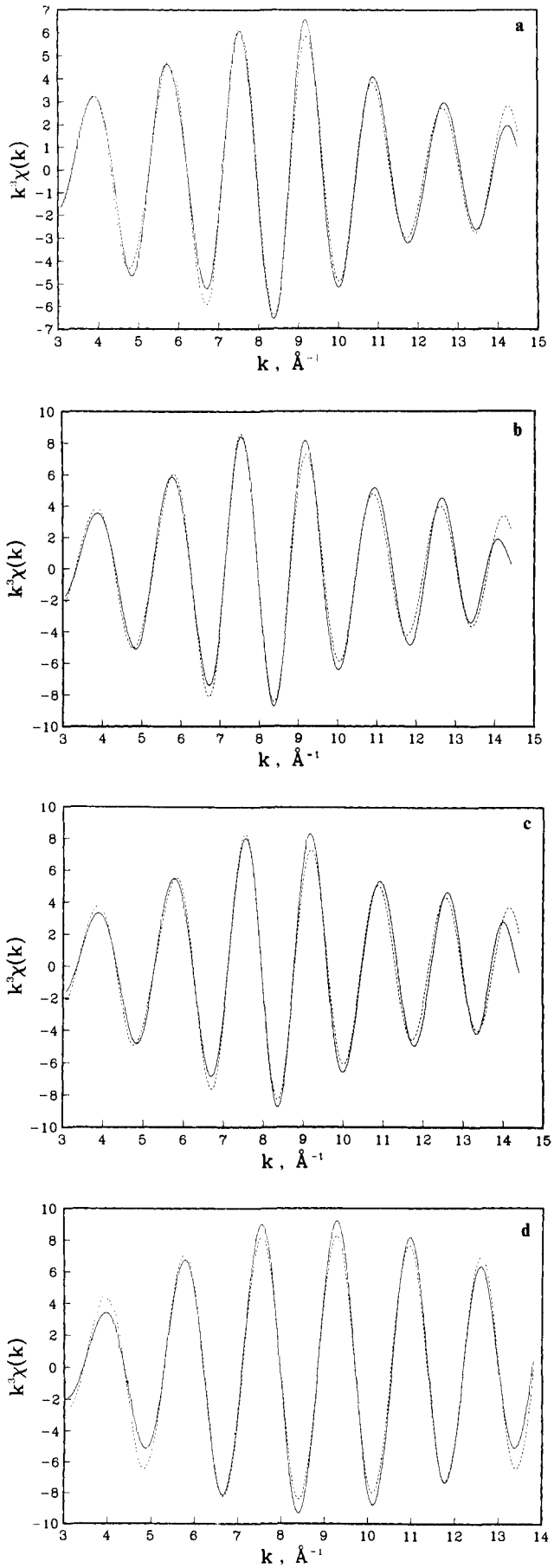

Figure 2. Fourier filtered $k^3\chi(k)$ vs. k tungsten L_3-edge EXAFS spectra (solid curves) and the nonlinear least-squares best fits (dashed curves), based on theoretical functions, to the filtered EXAFS of (a) **1**, (b) **3**, (c) **5**, and (d) **7**.

Table II. The Characteristic Energy Threshold Differences (ΔE_0*, eV), Debye–Waller Factors (σ*, Å), and Amplitude Reduction factors (S*) for the W L_3-Edge and the Fe K-Edge Transmission EXAFS of Complexes **1–4**, **6**, and **7**

		distance	coordination no.	
compd	term	ΔE_0*[a]	σ*	S*[b]
1	W–S	13.01 (13.36)	0.049	0.397
	W–Fe	5.65 (7.05)	0.073	0.344
1	Fe–S	7.57 (7.46)	0.054	0.480
	Fe–W	−1.38 (−4.37)	0.053	0.528
2	W–S			0.473
	W–Fe	5.71 (5.93)	0.070	0.443
2	Fe–S/Cl			0.483
	Fe–W	−5.10 (−3.20)	0.079	0.269
3	W–S	13.94 (13.43)	0.048	0.511
	W–Fe	4.16 (3.91)	0.070	0.522
3	Fe–S	5.73 (5.85)	0.042	0.378
	Fe–W	0.81 (−7.95)	0.061	0.301
	Fe–O	6.90 (5.37)	0.005	0.543
4	W–S	12.26 (12.13)	0.054	0.410
	W–Fe	2.38 (2.93)	0.053	0.441
4	Fe–S	7.82 (7.77)	0.053	0.453
	Fe–W	−3.87 (−6.41)	0.049	0.554
6	W–S	11.29 (11.27)	0.020	0.437
	W–Fe	6.62 (7.08)	0.071	0.401
6	Fe–S/Cl	6.92 (6.65)	0.065	0.416
	Fe–W	−3.71 (0.76)	0.071	0.478
7	W–S	7.12 (7.14)	0.028	0.480
		Average Values		
	W–S	11.52 (11.47)	0.050[c], 0.024[d]	0.451
	W–Fe	4.90 (5.38)	0.067	0.430
	Fe–S/Cl	7.01 (6.93)	0.054	0.442
	Fe–W	−2.65 (−4.23)	0.063	0.426

[a] The parenthetical values were obtained from the regression lines shown in Figures XVIII and XX (supplementary material) for comparison with the corresponding values for from restricted parameter curve fitting. The results from both treatments are in excellent agreement for the W–S and Fe–S/Cl terms, and larger differences (ca. 1–9 eV) are observed for the W–Fe and Fe–W terms. The discrepancies, which amount to ca. 0.025 Å for the Fe–W term of **3**, are due to different parameter cross sections of the multi-dimensional surfaces in the restricted-fit and best-fit least-squares refinements. The values obtained from the regression lines are more accurate representations of the curvature of the chi-square minimum surface in the best fit parameter correlation space than are the restricted fit values. Thus, the average ΔE_0* values (in parentheses) obtained from the distance correlation regression lines were used in the fine adjustment of the BFBT distances. [b] Calculated from the scale factors (B, Table III) obtained at the average characteristic σ* values and the known numbers of neighbors, according to $S^* = B/N$. [c] Average of **1**, **3**, and **4**. [d] Average of **6** and **7**.

This significant decrease in the Fe–W scattering component to the EXAFS of **1–6** is due to the shape of the tungsten backscattering amplitude envelope as a function of the photoelectron wavevector k. Figure 4 shows the theoretical amplitude functions[13] ($F_M(k)$, cf. eq 1) for M = W, Mo, and Fe over the range $1 \leq k \leq 15$ Å^{-1}. For $k \lesssim 5$ Å, the tungsten amplitude is small, and for $k \gtrsim 10$ Å^{-1} the $F_W(k)$ function rises steeply; backscattering by W is thus important only in the high k region of the EXAFS. The scattering amplitude for W is less than that for Mo (between $1 \lesssim k \lesssim 13$ Å^{-1}) and for Fe (between $3 \lesssim k \lesssim 11$ Å^{-1}), as shown in Figure 4. It is also clear from Figure 4 that the W backscattering amplitude function $F(k)$ has minima at ca. 5 and 10 Å^{-1} over the practical k range of importance (k = 3–15 Å^{-1}). From the comparison of W and Mo backscattering functions, it is now easy to understand that Fourier transformation of the available $k^3\chi(k)$ vs. k ($1 \lesssim k \lesssim 14.5$ Å^{-1}) Fe EXAFS data for **1–6** yields small peaks for the Fe–W backscattering (Figure 3a–c), whereas the peaks obtained for the Fe–Mo backscattering in the

(29) (a) Teo, B.-K.; Antonio, M. R.; Tieckelmann, R. H.; Silvis, H. C.; Averill, B. A. *J. Am. Chem. Soc.* **1982**, *104*, 6126. (b) Antonio, M. R.; Teo, B.-K.; Orme-Johnson, W. H.; Nelson, M. J.; Groh, S. E.; Lindahl, P. A.; Kauzlarich, S. M.; Averill, B. A. *J. Am. Chem. Soc.* **1982**, *104*, 4703. (c) Teo, B.-K.; Eisenberger, P.; Kincaid, B. M. *J. Am. Chem. Soc.* **1977**, *99*, 1735.

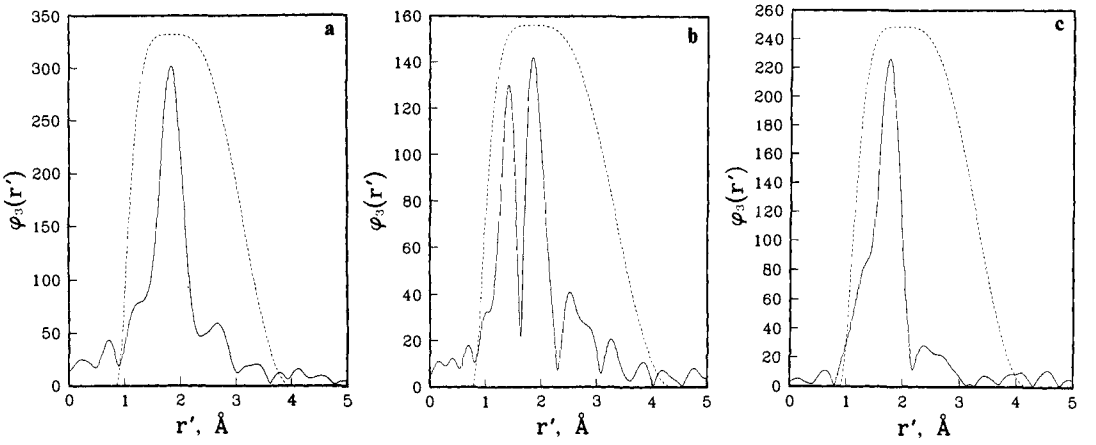

Figure 3. Fourier transforms (solid curves), $\phi_3(r')$ vs. r' (Å; before phase shift correction), of the background-subtracted $k^3\chi(k)$ vs. k iron K-edge transmission EXAFS data and filtering windows (dashed curves) for (a) **1**, (b) **3**, and (c) **5**.

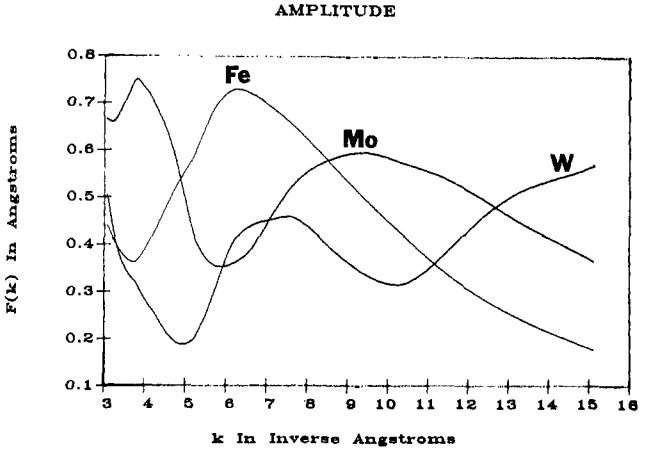

Figure 4. Theoretical backscattering amplitude functions (F_M; M = W, Mo, Fe) vs. photoelectron wavevector k.

analogous Mo–Fe–S clusters are much larger.[28,29a] Owing to the extremely small amplitude of the Fe–W component of the total EXAFS, an accurate determination of the number of tungsten neighbors from the Fe EXAFS of **1–6** is somewhat difficult (vide infra). In order to obtain accurate information concerning the Fe–W peak, one needs to extend the X-ray absorption measurements of the iron K-edge out to $k \gtrsim 18$ Å^{-1}.

The filtered $k^3\chi(k)$ vs. k EXAFS data of the clusters were fit with eq 1 with j = S, W for **1** and **4**; j = X, W where X = (S + Cl)/2 for **2** and **6**; and j = O, S, and W for **3**. The backscattering amplitude and phase functions for X were obtained by a simple point-by-point arithmetic-mean averaging of the corresponding functions[13,21] for S and Cl. The filtered $k^3\chi(k)$ spectrum of **5** was resolved into two components, $k^3\chi_S(K)$ and $k^3\chi_M(k)$ for Fe–S and Fe–W/Fe interactions, respectively, via a difference Fourier technique,[29] and fitted with one (j = S) and two term (j = W and Fe) contributions,[18a,22] respectively. The best-fit (BFBT) parameters (ΔE_0^P, r, σ, B) are listed in Table I; the fits are shown as the dashed curves in Figure 5a–c.[20b] The FABM results, using characteristic values listed in Table II, are tabulated in Table III.[30]

The Fe–S distances of **1–6** are ca. 0.01–0.02 Å longer than the corresponding Fe–S bond lengths in the Mo–Fe–S cluster analogues **1′–6′**.[28] The magnitude of the increases for the Fe–S distances in **1–6** are in line with the slight lengthening of the Fe–M

(30) The parameters and curvature of the best fit chi-square surface for the novel trinuclear trianion **5** with the proposed FeS_2FeS_2W core unit are consistent with those of the structurally characterized molybdenum analogue **5′** in which the iron atoms are in two distinct sites.[29a] Complex **5′** is thus a good model compound for **5** (better than any of **1–4** and **6**), and the characteristic parameters found for **5′**[28,29a] were applied to the Fe EXAFS of **5** for the FABM analysis. It should be noted that the slope (166 eV/Å) of the Fe–W distance correlation for **5**, which has two nonequivalent Fe sites, is substantially smaller than the average of 370 eV/Å for clusters **1–4** and **6**.

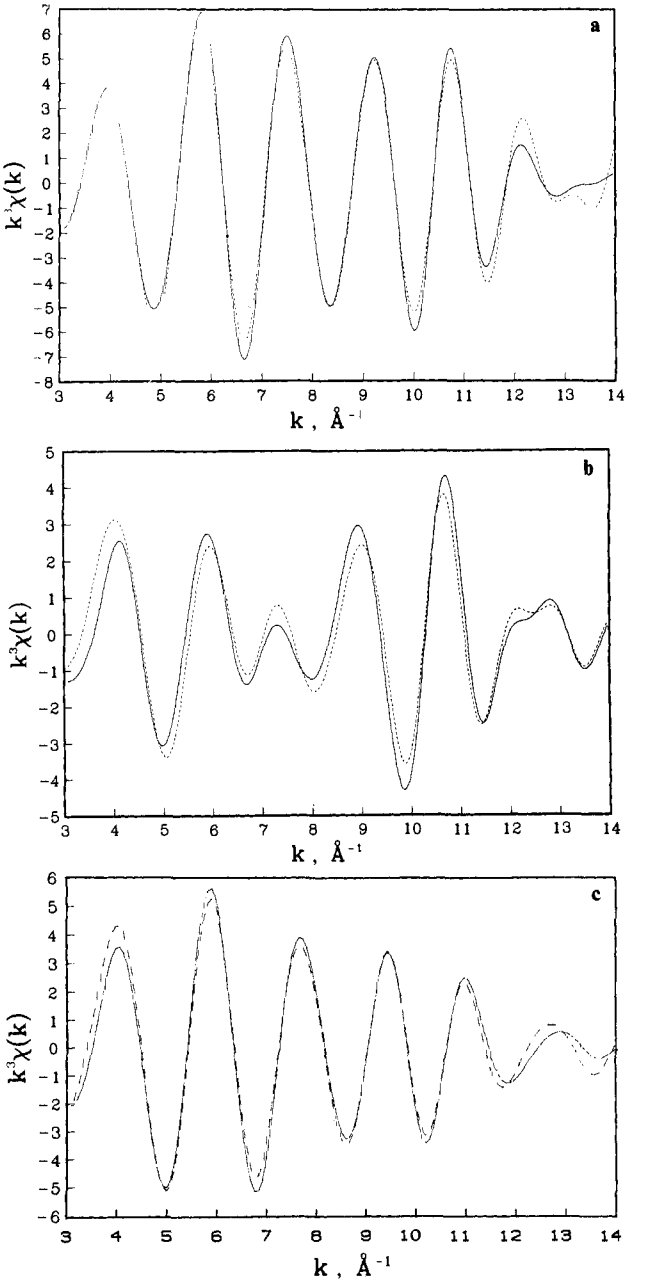

Figure 5. Fourier filtered $k^3\chi(k)$ vs. k iron K-edge EXAFS spectra (solid curves) and the nonlinear least-squares best fits (dashed curves), based on theoretical functions, to the filtered EXAFS of (a) **1**, (b) **3**, and (c) **5**.

Table III. The FABM Interatomic Distances (r, Å) and Coordination Numbers (N) with Estimated Standard Deviations (in Parentheses), Distance Adjustments (Δr, Å) to the BFBT Distances (Table I), and Scale Factors (B) for the W L_3-Edge and the Fe K-Edge Transmission EXAFS of Complexes **1**–**7**

		distance			coordination no.		
compd	term	Δr[a]	r	% error[b]	B[c]	N[d]	% error
1	W–S	−0.014	2.193 (12)	−0.4	1.588	3.5 (10)	−12.0
	W–Fe	0.068	2.764 (36)	−0.3	0.344	0.8 (5)	−20.0
1	Fe–S	−0.013	2.295 (17)	−0.1	1.919	4.3 (13)	8.5
	Fe–W	0.006	2.772 (35)	0.0	0.528	1.2 (9)	23.9
2	W–S	−0.016	2.192 (12)		1.893	4.2 (12)	4.9
	W–Fe	0.058	2.807 (44)	0.0	0.443	1.0 (7)	3.0
2	Fe–S/Cl	0.002	2.287 (18)		1.934	4.4 (15)	9.4
	Fe–W	0.060	2.804 (30)	−0.1	0.269	0.6 (4)	−36.9
3	W–S	−0.013	2.194 (12)	−0.4	2.046	4.5 (14)	13.4
	W–Fe	0.088	2.804 (51)	0.4	0.522	1.2 (9)	21.4
3	Fe–S	−0.040	2.311 (15)	0.2	0.757	1.7 (5)	−14.4
	Fe–W	−0.021	2.804 (40)	0.4	0.301	0.7 (5)	−29.3
	Fe–O	0.027[c]	1.889 (24)[e]	0.0	0.601[e]	1.9 (3)[e]	−4.3
4	W–S	−0.001	2.202 (12)	−0.2	1.642	3.6 (11)	−9.0
	W–Fe	0.044	2.761 (28)	0.3	0.441	1.0 (6)	2.6
4	Fe–S	−0.016	2.291 (17)	−0.2	1.811	4.1 (13)	2.4
	Fe–W	0.002	2.758 (37)	0.2	0.554	1.3 (10)	30.0
5	W–S	−0.018	2.199 (11)		2.058	4.6 (14)	14.1
	W–Fe	0.069	2.801 (56)		0.495	1.2 (8)	15.1
5	Fe–S	0.003[f]	2.254 (20)[f]		1.561[f]	3.9 (9)[f]	−2.7
	Fe–W	0.010[f]	2.796 (20)[f]		0.154	0.4 (3)	−27.7
	Fe–Fe	−0.019[f]	2.783 (26)[f]		0.181[f]	0.7 (2)[f]	−31.4
6	W–S	−0.012	2.210 (10)	0.0	1.748	3.9 (10)	−3.1
	W–Fe	0.033	2.794 (44)	−0.3	0.802	1.9 (13)	−6.7
6	Fe–S/Cl	0.015	2.281 (24)	0.1	1.666	3.8 (12)	−5.8
	Fe–W	−0.039	2.782 (36)	−0.7	0.478	1.1 (7)	12.2
7	W–S	−0.023	2.187 (10)	0.8	1.920	4.3 (10)	6.4

[a] Calculated according to $\Delta r = (\Delta E_0^* - \Delta E_0^P)/a_1$, where ΔE_0^* was the average characteristic energy threshold difference for the term (Table II), ΔE_0^P was the BFBT energy threshold difference (Table I), and a_1 was the slope of the distance correlation (Tables I and II, supplementary material). [b] See Table I for the corresponding crystallographic distances. [c] Calculated according to $B = b_0 + b_1\sigma^* + b_2\sigma^{*2}$ where σ^* was the average characteristic Debye–Waller factor for the term (Table II) and b_0, b_1, and b_2 were the regression coefficients for the amplitude correlation (Tables I and II, supplementary material). [d] Calculated according to $N = B/S^*$, where S^* was the average characteristic amplitude reduction factor for the term (Table II). [e] Distance correction,[a] scale factor,[c] and coordination number[d] were calculated with $\Delta E_0{}^*{}_O = 5.50$ eV, $\sigma^*{}_O = 0.031$ Å, and $S^*{}_O = 0.314$, respectively, obtained from the iron transmission EXAFS analysis[28] of the model compound $(Et_4N)_2[(C_6H_5O)_2FeS_2MoS_2]$. [f] Distance corrections[a] ($\Delta E_0{}^*{}_W = 16.89$ and $\Delta E_0{}^*{}_{Fe} = 15.24$ eV), scale factors[c] ($\sigma^*{}_S = 0.065$ and $\sigma^*{}_{Fe} = 0.061$ Å), and coordination numbers[d] ($S^*{}_S = 0.401$ and $S^*{}_{Fe} = 0.264$) were based upon the characteristic parameters obtained from the iron transmission EXAFS analysis[28] of the model compound $(Et_4N)_3[(p\text{-}CH_3C_6H_4S)_2FeS_2FeS_2MoS_2]$.

Table IV. The Average Terminal W–S and Fe–S/Cl and Bridging W–S and Fe–S Interatomic Distances (r, Å) as Estimated from the EXAFS-Determined Debye–Waller Factors (σ, Å) for the W L_3-Edge and the Fe K-Edge Transmission EXAFS of Complexes **1**–**7**, along with Available Single-Crystal X-ray Diffraction Results

		EXAFS						diffraction[a]			
compd	term	σ_{bf}[b]	σ_{stat}[c]	δr[d]	r[e]	r_m[f]	r_n[f]	σ_{calcd}[g]	σ_{stat}[h]	r_b	r_t
1	W–S	0.048 (14)	0.039	0.078	2.193 (12)	2.232	2.154	0.051	0.043	2.245 (2)	2.159 (2)
	Fe–S	0.055 (18)	0.032	0.063	2.295 (7)	2.327	2.264	0.046	0.011	2.288 (2)	2.306 (2)
2	W–S	0.045 (10)	0.035	0.070	2.192 (12)	2.227	2.157				
	Fe–S/Cl	0.061 (16)	0.041	0.082	2.287 (18)	2.328	2.246				
3	W–S	0.049 (16)	0.040	0.080	2.194 (12)	2.234	2.154	0.050	0.041	2.241 (3)	2.164 (7)
	Fe–S	0.035 (34)	0	0	2.311 (15)			0.045	0.003	2.307 (3)	
4	W–S	0.052 (17)	0.044	0.088	2.202 (12)	2.246	2.158	0.058	0.051	2.255 (7)	2.157 (8)
	Fe–S	0.053 (17)	0.028	0.056	2.291 (17)	2.319	2.263	0.052	0.026	2.270 (7)	2.319 (9)
5	W–S	0.045 (20)	0.035	0.070	2.199 (11)	2.234	2.164				
	Fe–S	0.074 (21)	0.059	0.118	2.254 (20)	2.313	2.195				
6	W–S	0.020 (20)	0	0	2.210 (10)			0.028	0.005	2.209 (5)	
	Fe–S/Cl	0.063 (20)	0.044	0.088	2.281 (24)	2.325	2.237	0.063	0.044	2.320 (6)	2.233 (6)
7	W–S	0.026 (22)	0	0	2.187 (10)			0.029	0.007		2.165 (10)

[a] The single-crystal X-ray diffraction results were obtained from ref 8a for **1** and **3** and ref 10a, 10c, and 11b for **4**, **6**, and **7**, respectively. [b] The least-squares refined BFBT Debye–Waller factor with estimated standard deviation (Table I). [c] Calculated according to $\sigma_{stat} = (\sigma_{bf}{}^2 - \sigma_{vib}{}^2)^{1/2}$, where $\sigma_{vib} = 0.028$ Å for the W–S terms and $\sigma_{vib} = 0.045$ Å for the Fe–S/Cl terms. [d] Calculated according to $\delta r = \sigma_{stat}(m + n)/(mn)^{1/2}$, where $m = n = 2$ for the W–S terms of **1**–**5** and $m = n = 2$ for the Fe–S/Cl terms of **1**, **2**, **4**, **5**, and **6**. If $m = 1$, $n = 3$ for the Fe–S term of **5**, $\delta r = 0.136$, $r_m = 2.356$, $r_n = 2.220$ Å. [e] Average interatomic distance with estimated standard deviation from the FABM treatment (Table III). [f] Calculated according to $r_n = r + n\delta r/(m + n)$ and $r_n = r - m\delta r/(m + n)$. [g] Calculated according to $\sigma_{calcd} = (\sigma_{stat}{}^2 + \sigma_{vib}{}^2)^{1/2}$, where σ_{vib} was 0.028 and 0.045 Å for the W–S and Fe–S/Cl terms, respectively, and σ_{stat} was obtained from the diffraction data. [h] Calculated according to $\sigma_{stat} = [\sum_{i=1}^{N}(r_i - r)^2/N]^{1/2}$, where r is the mean crystallographical distance.

distances observed upon replacement of molybdenum by tungsten in **1**–**6**.[4,6,7]

The best-fit Debye–Waller factors (σ_{bf}) for the Fe–S/Cl bonds of complexes **1**–**6** provide an accurate measure of the spread in the Fe–S/Cl distances (δr) from which average terminal and bridging interatomic distances (r_m, r_n) can be determined. The results are tabulated in Table IV. For comparison, the corresponding Debye–Waller factors (σ_{calcd}, σ_{stat}) and average bridging and terminal distances (r_b, r_t) from X-ray crystallography are also listed in Table IV. For both **1** and **4**, the terminal Fe–S distances

are longer than the bridging Fe–S distances, whereas for **6** the terminal Fe–Cl distance is shorter than the bridging Fe–S distance.[10c] The terminal Fe–Cl and bridging Fe–S bond lengths in $[Cl_2FeS_2WS_2]^{2-}$ (**2**), for which a twofold static disorder results only in average M–X distances being obtainable from single-crystal X-ray crystallography,[7,9a] are reasonably expected to be in line with those of **6**. Thus, the EXAFS resolved distances r_m = 2.328 Å and r_n = 2.246 Å for **2** are attributed to bridging Fe–S and terminal Fe–Cl backscatterings, respectively. For the structurally yet-unknown **5**, δr = 0.118, r_m = 2.313, and r_n = 2.195 Å if we assume that the four Fe–S distances exo to the Fe_2S_2 unit are longer than the four Fe–S distances connecting the two irons, in analogy to the Mo analogue[29a] **5′** (m:n = 2:2). Another way of partitioning the Fe–S distances is to assume that the two terminal Fe–S distances are longer than the six bridging Fe–S distances (m:n = 1:3); then we obtain δr = 0.136, r_m = 2.356, and r_n = 2.220 Å. Though both sets are consistent with the EXAFS data, the former is more reasonable by comparison with the Mo analogue **5′** (the corresponding crystallographic values are δr = 0.088, r_m = 2.299, and r_n = 2.211 Å[29a]). The EXAFS and diffraction results[4,6,7] (Table IV) indicate that for clusters **1–4** and **6** the mean bridging Fe–S bonds are ca. 0.01–0.03 Å longer than those for the corresponding Mo–Fe–S clusters, whereas the mean terminal Fe–S/Cl bond lengths for the W–Fe–S and Mo–Fe–S clusters are nearly identical.

Conclusions

The W L_3-edge and Fe K-edge transmission EXAFS spectra of six W–Fe–S clusters (**1–6**) containing the WS_2Fe core have been measured. The results are compared with the corresponding Mo analogues (**1′–6′**). Overall, the core dimensions of the W–Fe–S and Mo–Fe–S clusters are virtually equivalent; only small increases are observed for the W–Fe and bridging Fe–S distances of **1–6** vs. the corresponding Mo–Fe and bridging Fe–S distances in the Mo–Fe–S cluster analogues, and the parameter correlation curves for the EXAFS data of the Mo–Fe–S and W–Fe–S clusters exhibit very similar trends. Finally, the terminal M–S/Cl and bridging M–S interatomic distances were accurately determined from the average M–S/Cl distances in **1–6** and the best-fit Debye–Waller factors.

The most important finding of the present study is the near-absence of the Fe–W peak in the Fourier transform of the iron EXAFS of the title compounds. In sharp contrast to the principles of X-ray diffraction, the generally held notion that heavier neighboring atoms are stronger backscatterers than lighter atoms obviously does not always hold in EXAFS spectroscopy. This type of information loss in EXAFS spectroscopy is explained by the fact that the tungsten backscattering amplitude profile has two minima at ca. 5 and 10 $Å^{-1}$ in the k region of practical importance. To enhance the tungsten EXAFS signal, it may be necessary to extend the data to high k regions or to minimize the Debye–Waller factor by performing the experiments at low temperature.

It is important to emphasize that other heavy atoms, such as the third row transition metals, that have minima in their backscattering amplitude functions may also be weak EXAFS backscatterers. As such, the associated information loss decreases their suitability for use as EXAFS candidates for heavy-atom substitution studies, especially for dilute biological systems.

Acknowledgment. This research was supported in part by grants to B.A.A. from the USDA/SEA Competitive Grants Office (5901-0418-8-0175-0). B.A.A. was an Alfred P. Sloan Foundation Fellow, 1981–1985. We thank Drs. D. Coucouvanis and H. C. Silvis and R. H. Tieckelmann for providing the compounds studied herein, and we are also indebted to S. M. Kauzlarich for her assistance. We thank the staff at CHESS for their assistance.

Registry No. 1, 73493-03-5; **2**, 76483-99-3; **3**, 95763-56-7; **4**, 73493-06-8; **5**, 95763-57-8; **6**, 73621-81-5; **7**, 14916-78-0.

Supplementary Material Available: Figures I–XIII (the raw X-ray absorption data in the form μX vs. E, in eV, and the background-subtracted W and Fe EXAFS spectra, $k^3\chi(k)$ vs. k for **1–7**), Figures XIV and XV (Fourier transforms of the background-substracted W and Fe EXAFS spectra for **2**, **4**, and **6**), Figures XVI and XVII (the Fourier filtered $k^3\chi(k)$ vs. k W and Fe EXAFS data and the nonlinear least-squares best fits, based on theoretical functions, to the filtered EXAFS of **2**, **4**, and **6**), Figures XVIII–XXI (parameter correlations, ΔE_0 vs. Δr, and B vs. σ, encountered in the nonlinear least-squares curve fitting to the filtered W and Fe EXAFS data of **1–7**), and Tables I and II (linear least-squares regression coefficients for the correlation curves obtained from the curve fitting to the W and Fe EXAFS data of **1–7**) (51 pages). Ordering information is given on any current masthead page.